

Superimposed Pilot-based Channel Estimation for RIS-Assisted IoT systems Using Lightweight Network

Chaojin Qing

qingchj@mail.xhu.edu.cn

Xihua University

Wenquan Hu

Xihua University

Li Wang

Xihua University

Guowei Ling

Xihua University

Zhiying Liu

Xihua University

Xi Cai

Xihua University

Jiafan Wang

Xihua University

Research Article

Keywords: Channel estimation, Internet of Things, superimposed pilot, reconfigurable intelligent surface, lightweight neural networks

Posted Date: July 12th, 2023

DOI: <https://doi.org/10.21203/rs.3.rs-3137264/v1>

License:   This work is licensed under a Creative Commons Attribution 4.0 International License.

[Read Full License](#)

Additional Declarations: No competing interests reported.

Version of Record: A version of this preprint was published at Wireless Personal Communications on March 28th, 2024. See the published version at <https://doi.org/10.1007/s11277-024-10923-9>.

Superimposed Pilot-based Channel Estimation for RIS-Assisted IoT systems Using Lightweight Network

Chaojin Qing^{1*}, Wenquan Hu¹, Li Wang¹, Guowei Ling¹,
Zhiying Liu¹, Xi Cai¹, Jiafan Wang¹

¹School of Electrical Engineering and Electronic Information,
Xihua University, Chengdu, 610039, China.

*Corresponding author(s). E-mail(s): qingchj@mail.xhu.edu.cn;

Abstract

Channel estimation (CE) in Internet of Things (IoT) systems faces challenges of low spectral efficiency, high energy consumption, and blocked propagation paths. To address these issues, this paper proposes a superimposed pilot-based CE scheme with reconfigurable intelligent surface (RIS) assistance. The pilot signal is superimposed on the uplink user data to improve spectral efficiency and reduce user equipment (UE) energy consumption. RIS is introduced to enhance communication robustness in the complex propagation environments. At the base station (BS), dedicated lightweight neural networks (NNs) are developed for CE and symbol detection (SD) to alleviate computational complexity and processing delay. The limited learning ability of these lightweight NNs is addressed by employing conventional CE and SD methods for initial feature extraction. This enables the NNs to learn along with the extracted features, reducing the required training set size. The proposed scheme improves spectral efficiency, reduces energy consumption, computational complexity, and processing delay, while enhancing the performance of both normalized mean square error (NMSE) of CE and the bit error rate (BER) of SD. Simulation results demonstrate the robustness of the proposed method against various parameter settings.

Keywords: Channel estimation, Internet of Things, superimposed pilot, reconfigurable intelligent surface, lightweight neural networks.

1 Introduction

As the cornerstone of the future Internet of Things (IoT) connectivity, the evolution of fifth-generation (5G) and sixth-generation (6G) networks has attracted consistent attention in the application of IoT systems. For example, intelligent buildings connected with the internet to manage different devices [1], smart health care and intelligent driving proposed in [2], and home automation put forward by [3], etc. In these IoT systems, channel estimation (CE) plays critical roles, such as to overcome channel time variation [4] and adjust to an affordable transmission power using appropriate modulation and coding methods [5].

Owing to the importance of CE for the IoT systems, numerous studies have investigated the CE [4], [6]–[9]. However, there is still room for improvement in terms of spectral efficiency and energy consumption reduction in existing CE schemes [4] and [6]–[9]. Conventional pilot-based CE approaches used in IoT systems, such as those in [4] and [6]–[9], require additional transmission resources for pilot signals, resulting in low spectral efficiency. Moreover, energy consumption is a critical concern in IoT systems. For instance, [10] aims to extend the battery lifetime of user equipment (UE) up to ten years. The time-division mode for transmitting pilots and data separately significantly increases energy consumption and makes it challenging to achieve the desired system targets. To address this issue, the authors in [11] employed the superimposed transmission to improve the efficiencies of spectrum and energy. Inspired by the superimposed pilot strategy, we propose a CE solution for IoT systems based on superimposed pilots. This approach allows for improved spectral efficiency and reduced energy consumption.

In addition to the challenges posed by low spectral efficiency and high energy consumption, IoT communication usually faces the issue of blocked propagation in complex environments, such as in industrial IoT (IIoT) scenarios [4]. Enhancing the robustness of the communication link is crucial for IoT systems. Reconfigurable intelligent surface (RIS) offers a promising solution to address the problem of blocked propagation [12]. The RIS is an artificial panel comprising a large array of low-cost passive scattering elements that can manipulate wireless signals by adjusting their amplitude and phase shift [12]. Unlike conventional amplify-and-forward relays, RIS elements consume minimal energy [13]. Integrating RIS into IoT systems has been recognized as a transformative approach to convert passive wireless environments into active and reconfigurable ones, providing environmental intelligence for various communication objectives [14]. Furthermore, RIS can enhance system throughput by at least 40 percent and system coverage by one-third [15, 16]. Leveraging RIS in the context of superimposed pilot-based CE for IoT systems is a highly desirable approach to address the challenges of blocked propagation. To our best knowledge, this approach has not been explored in existing literature, highlighting the novelty of our proposed work.

Recently, deep learning (DL) has made a significant breakthrough in advanced information processing and computer vision [17]. In [18], DL is characterized by its ability to learn the mapping between input and output through training data samples, which enables the development of a model structure for predicting system output. Potential applications of DL in the physical layer have been increasingly recognized due

to the new features of future communications, such as complex scenarios of unknown channel models and precise processing requirements [17]. Specially, DL-based CE in RIS-assisted communication systems has also aroused extensive research interest. In [19], two convolutional neural networks (CNN)-based CEs are developed for approximating the minimum mean square error (MMSE)-based CE solution. An enhanced extreme learning machine (ELM)-based CE is proposed in [20] to facilitate the estimation accuracy. In [21], to improve the pilot-based least-squares (LS) estimation, an untrained deep neural network (NN) based on the deep image prior network is developed for CE. However, DL-based superimposed CE in RIS-assisted communication systems has not been investigated, which is particularly important for an IoT system to reduce the energy consumption with high spectral efficiency. In addition, the size of training set for DL-based superimposed CE is usually large, otherwise NNs cannot get enough information to explore the underlying relationship of wireless channels.

To address the challenges of energy consumption, blocked propagation, and CE accuracy in IoT systems, we propose the superimposed pilot-based CE for RIS-assisted IoT systems with lightweight networks. The main contributions of our work are summarized as follows:

1. We integrate the superimposed pilot-based and RIS-assisted modes into the CE of IoT systems to alleviate the issues of spectral efficiency and energy-consuming. On the one hand, by employing the superimposed pilot-based mode, the UE energy consumption is reduced and the system spectral efficiency is improved. On the other hand, the robustness of the communication link is enhanced with the assistance of RIS. Especially, the combinations of superimposed pilot-based mode and RIS assistance further reduce the energy consumption, and thus prolong the battery life of UE. Besides, superimposed pilot-based method can effectively alleviate the problem of channel changes frequently and refine the estimation performance. As far as we know, with prolonged battery life of UE and enhanced spectral efficiency of the IoT system, the issue of improving the accuracy of the CE has not been well addressed in [10, 22]. Therefore, it is beneficial to study the superimposed pilot-based CE for RIS-assisted systems.
2. We develop two dedicated lightweight NNs to reduce the computational complexity and processing delay for the CE and symbol detection (SD) at the base station (BS). To remedy the limited learning capacity of lightweight NNs, the initial features are highlighted by employing conventional CE and SD methods (non-NN solutions) to perform feature extraction, and the lightweight networks are oriented to learn along with the highlighted initial features. From the perspective of feature fusion (by fusing the non-NN and NN-based solutions), the performance of CE and SD can be improved. Due to the assistance of non-NN solutions, both the CE and SD networks can be lightweight, which allows their training set to be reduced as well. The computational complexity of lightweight NN is reduced, saving computational resources and processing delays.
3. With the reduced computational complexity and processing delay, we further improve the normalized mean square error (NMSE) and bit error rate (BER) performances at the BS. For CE, we exploit the learning ability of the developed CE network according to de-noising (suppress the superimposed interference and noise)

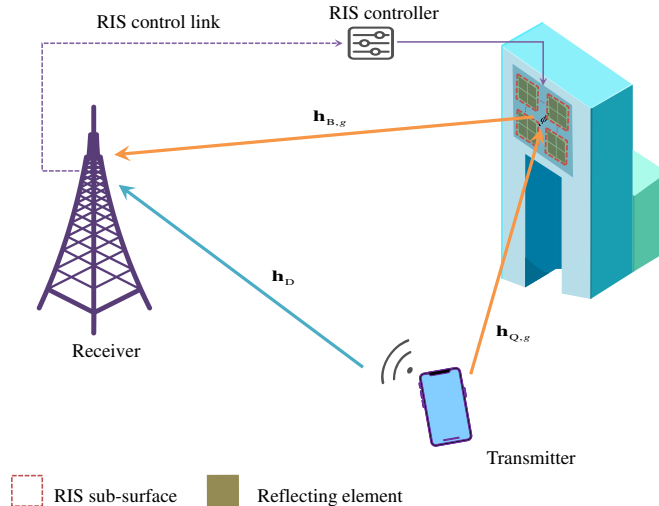


Fig. 1 An illustration of RIS-assisted OFDM communication in the uplink.

and feature extraction, which alleviates the influence of superimposed interference. The improved CE refines NMSE performance, and thus improves the accuracy of subsequent SD. Besides, the developed fusion network captures additional features for SD so that improves the BER performance effectively at the BS.

The remainder of this paper is structured as follows: In Section 2, we present the system model. The proposed method is elaborated in Section 3. The computational complexity and running time is analyzed in Section 4, and followed by numerical results in Section 5. Finally, Section 6 concludes our work.

Notations: Bold face lower case and upper case letters represent vector and matrix, respectively. $(\cdot)^T$ is the transpose. \odot stands for the Hadamard product. $\text{diag}\{\cdot\}$ is the diagonal matrix. $\text{Re}(\cdot)$ and $\text{Im}(\cdot)$ represent the real and imaginary parts of complex numbers, respectively.

2 System Model

As shown in Fig. 1, we consider a frequency-selective Rician fading RIS-assisted IoT system with orthogonal frequency division multiplexing (OFDM) modulation. In Fig. 1, supposing that the propagation path is blocked by buildings, the RIS is installed on the surface of the building to alleviate this issue. The composite channel frequency response (CFR) of the transmitter-receiver link is denoted as \mathbf{h}_D . Additionally, the aggregated CFRs of the RIS-receiver link and the transmitter-RIS link related to the g -th sub-surface are represented by $\mathbf{h}_{B,g}$ and $\mathbf{h}_{Q,g}$, respectively. The RIS comprises numerous passive reflecting elements, and to reduce the complexity and training overhead of CE, adjacent elements form sub-surfaces with shared reflection coefficients in the RIS configuration [23]. Besides, the RIS control link is used to adjust the phase shift. This system considers N sub-carriers and assumes the length of channel impulse

response (CIR) L is shorter than the length of cyclic prefix (CP) L_{CP} , i.e., $L < L_{CP}$ [6], [23], to mitigate inter-symbol interference (ISI). The received frequency-domain signal at the BS is denoted as

$$\mathbf{y} = \sqrt{\lambda P} \mathbf{h} \odot \mathbf{x}_p + \sqrt{(1-\lambda)P} \mathbf{h} \odot \mathbf{x}_d + \mathbf{w}, \quad (1)$$

where $\lambda \in [0, 1]$ is the coefficient of power proportional, P stands for the total transmitting power. $\mathbf{h} = [h_1, h_2, \dots, h_N]^T$ represents the wireless CFR between the receiver and transmitter. $\mathbf{x}_p \in \mathbb{C}^{N \times 1}$ and $\mathbf{x}_d \in \mathbb{C}^{N \times 1}$ denote the superimposed pilot and the modulated signal, respectively. $\mathbf{w} \in \mathbb{C}^{N \times 1}$ follows a circularly symmetric complex Gaussian (CSCG) distribution with zero mean and a specific variance σ_w^2 .

The composite CFR linking the receiver and transmitter is expressed as [23]

$$\mathbf{h} = \mathbf{h}_D + \mathbf{H}_{QB} \boldsymbol{\phi}, \quad (2)$$

where $\mathbf{h}_D \in \mathbb{C}^{N \times 1}$ denotes the CFR of the transmitter-receiver link, and $\mathbf{H}_{QB} \in \mathbb{C}^{N \times M}$ represents the cascaded CFR of the transmitter-RIS-receiver link. $\boldsymbol{\phi} = [\phi_1, \phi_2, \dots, \phi_G]^T$ stands for the vector of RIS phase-shift, which is given by

$$\phi_g = \alpha_g e^{j\theta_g}, \quad g = 1, \dots, G, \quad (3)$$

where $\theta_g \in [0, 2\pi]$ represents the phase shift associated with the g -th sub-surface, and G is the number of sub-surfaces. To streamline hardware design and optimize RIS reflection power, according to [20], we fix $\alpha_g = 1, \forall g = 1, \dots, G$, while only manipulating the phase shift θ_g .

By denoting $\mathbf{H}_{QB} = [\mathbf{h}_{QB,1}, \mathbf{h}_{QB,2}, \dots, \mathbf{h}_{QB,G}]$, $\mathbf{h}_{QB,g}$ is expressed as

$$\mathbf{h}_{QB,g} = \mathbf{h}_{Q,g} \odot \mathbf{h}_{B,g}, \quad (4)$$

where $\mathbf{h}_{Q,g} \in \mathbb{C}^{N \times 1}$ represents the aggregated CFR of the transmitter-RIS link, while $\mathbf{h}_{B,g} \in \mathbb{C}^{N \times 1}$ denotes the aggregated CFR of the RIS-receiver link, both in relation to the g -th sub-surface.

According to (1), (2) and (4), the received frequency-domain signal at the receiver is rewritten as

$$\mathbf{y} = \left(\mathbf{h}_D + \sum_{g=1}^G \mathbf{h}_{Q,g} \phi_g \odot \mathbf{h}_{B,g} \right) \odot \left(\sqrt{\lambda P} \mathbf{x}_p + \sqrt{(1-\lambda)P} \mathbf{x}_d \right) + \mathbf{w}. \quad (5)$$

The received signal \mathbf{y} is processed by LS estimation and zero-forcing (ZF) equalization at the receiver, aiming to improve the accuracy of initial estimation features and alleviate the learning burden on the network.

In this paper, to save bandwidth resources and energy-consuming [24], we adopt the method of superimposed pilot for CE and SD. Specifically, we propose two dedicated lightweight networks, namely LwCE-Net and FuSD-Net, which are designed to enhance the performance of CE and SD, respectively. Different from the conventional methods,

e.g., the MMSE CE and MMSE SD, non-NN and lightweight NN-based approaches are integrated into our work, in which the LwCE-Net and FuSD-Net are embedded into conventional methods to obtain network lightweight and cooperatively improve the performance of CE and SD.

3 Superimposed Pilot-based Channel Estimation

This paper presents a three-step process for signal transmission. Firstly, the pilot signal \mathbf{x}_p and modulated signal \mathbf{x}_d are superimposed at the UE. Secondly, an inverse fast Fourier transform (IFFT) is performed, followed by the addition of CP operations. Thirdly, the signal propagates through the wireless channel. At the receiver, the received signal \mathbf{y} is obtained by removing the CP and applying fast Fourier transform (FFT) operations. Subsequently, the lightweight NN utilizes LS estimation to emphasize the initial CE features. Since a lightweight NN possesses very limited learning ability, the highlighted initial features orient the learning of LwCE-Net and thus improve the effectiveness of CE. Similarly, the developed FuSD-Net is also a lightweight network and thus needs to extract the initial equalization features. In this paper, the ZF equalization is utilized as a feature extractor for initial equalization features $\hat{\mathbf{s}}_{ZF}$. Using initial equalization feature $\hat{\mathbf{s}}_{ZF}$, the coarse data $\hat{\mathbf{s}}_d$ is obtained by cancelling the superimposed pilot. Then, the coarse data $\hat{\mathbf{s}}_d$ and the received signal \mathbf{y} are fed into the FuSD-Net to produce the detected symbol $\tilde{\mathbf{s}}_{FuSD}$.

Section 3.1 focuses on the initial feature extraction process for LwCE-Net, which is presented in Section 3.2 as a dedicated lightweight NN designed to enhance CE. The subsequent Section 3.3 discusses the initial feature extraction approach for FuSD-Net. In Section 3.4, we introduce FuSD-Net, a fusion learning-based lightweight NN specifically developed for SD. Lastly, Section 3.5 provides a comprehensive explanation of the online deployment process.

3.1 Initial CE Feature Extraction

With the received signal \mathbf{y} , the initial features of CE are extracted by LS estimation and used as the input of the LwCE-Net. By using the LS estimation, the initial CFR $\hat{\mathbf{h}}_{LS} \in \mathbb{C}^{N \times 1}$ is given by

$$\hat{\mathbf{h}}_{LS} = \left[\frac{y(1)}{x_p(1)}, \frac{y(2)}{x_p(2)}, \dots, \frac{y(N)}{x_p(N)} \right]^T, \quad (6)$$

where $y(n)$ and $x_p(n)$, $n = 1, 2, \dots, N$, are the received signal and transmitted pilots, respectively. The extracted feature, i.e., $\hat{\mathbf{h}}_{LS}$, is employed for subsequent enhancement of CE.

3.2 LwCE-Net based CE method

In order to obtain refined CE features that go beyond conventional estimation perspectives, we propose LwCE-Net, a lightweight and effective neural network. Then,

a certain estimation feature, called refined estimation feature $\tilde{\mathbf{h}}_{\text{CE}}$, is captured through LwCE-Net to complement the initial estimation feature $\hat{\mathbf{h}}_{\text{LS}}$.

3.2.1 LwCE-Net Architecture

According to [25], the parameter settings of LwCE-Net, e.g., layer depth, layer width, and activation function, are still a challenge in the NN. Through extensive experimental simulations and careful performance tradeoffs, we determine that the LwCE-Net consists of \mathcal{L} layers. Table 1 summarizes the LwCE-Net’s architecture, which is described in detail below.

To mitigate overfitting and enhance convergence speed in LwCE-Net [26], we apply batch normalization (BN) to the input layer. To address the issue of gradient vanishing [27], we utilize the rectified linear unit (ReLU) activation function ($f_a(x) = \max(0, x)$) in the hidden layers. These parameter choices in LwCE-Net contribute to the refinement of estimation performance.

Table 1
Architecture of LwCE-Net and FuSD-Net.

Layer	Input		Hidden 1		Hidden 2		Output	
	LwCE	FuSD	LwCE	FuSD	LwCE	FuSD	LwCE	FuSD
Batch normalization	✓	✓	×	×	×	-	×	×
Neuron number	$2N$	$4N$	$6N$	$8N$	$4N$	-	$2N$	$2N$
Activation function	-	-	ReLU	ReLU	ReLU	-	Linear	Linear

To enable the real-valued LwCE-Net, the complex variable $\hat{\mathbf{h}}_{\text{LS}} \in \mathbb{C}^{N \times 1}$ is transformed into a real-valued value $\tilde{\mathbf{h}}_{\text{LS}} \in \mathbb{R}^{2N \times 1}$ through the utilization of Eq. (7), which is expressed as,

$$\tilde{\mathbf{h}}_{\text{LS}} = \left[\text{Re} \left(\hat{\mathbf{h}}_{\text{LS}}^T \right), \text{Im} \left(\hat{\mathbf{h}}_{\text{LS}}^T \right) \right]^T. \quad (7)$$

Next, the entries of $\tilde{\mathbf{h}}_{\text{LS}}$ form the inputs of LwCE-Net. Via the LwCE-Net, the refined estimation feature, denoted as $\tilde{\mathbf{h}}_{\text{CE}} \in \mathbb{R}^{2N \times 1}$, is given by

$$\tilde{\mathbf{h}}_{\text{CE}} = f_{\text{CE}} \left(\tilde{\mathbf{h}}_{\text{LS}}, \mathbf{\Lambda}_{\text{CE}} \right), \quad (8)$$

where $f_{\text{CE}}(\cdot)$ and $\mathbf{\Lambda}_{\text{CE}}$ are the LwCE-Net operation and its network parameters, respectively. By referring to Eq. (8), we enhance the performance of CE without relying on second-order channel statistics.

3.2.2 Training and Deployment

A comprehensive dataset is collected to train the LwCE-Net. Specifically, the generation of these data samples is shown below.

The training set is represented by $\left\{ \tilde{\mathbf{h}}_{\text{LS}}, \tilde{\mathbf{h}}_{\text{Label}} \right\}$. In this paper, the channel which is characterized by frequency-selective fading, denoted as $\mathbf{h}_{\text{Label}}$, is obtained through

Algorithm 1 Fusion learning-based CE and SD

Input: Initial estimation $\tilde{\mathbf{h}}_{\text{LS}}$, training learning rate of LwCE-Net: γ_1 .
Training learning rate of FuSD-Net: γ_2 .
Batch size: ν , number of gradsteps for LwCE-Net: G_{CE} .
Number of gradsteps for FuSD-Net: G_{FuSD} .

Output: Refined detection $\tilde{\mathbf{s}}_{\text{FuSD}}$.

Training phase:

- 1: Randomly initialize the network parameters Θ_{CE} and Θ_{FuSD} .
- 2: Generate the training set $\{\tilde{\mathbf{h}}_{\text{LS}}, \tilde{\mathbf{h}}_{\text{Label}}\}$ and $\{\tilde{\mathbf{s}}_{\text{in}}, \tilde{\mathbf{x}}_{\text{d}}\}$.
- 3: **for** $t = 1, \dots, G_{\text{CE}}$ **do**
- 4: Randomly select ν training samples from $\{\tilde{\mathbf{h}}_{\text{LS}}, \tilde{\mathbf{h}}_{\text{Label}}\}$ as the training batch.
- 5: Update Θ_{CE} by using the Adam algorithm (learning rate γ_1) to minimize $\text{Loss}_{\text{LwCE-Net}}$
- 6: **end for**
- 7: **for** $t = 1, \dots, G_{\text{FuSD}}$ **do**
- 8: Randomly select ν training samples from $\{\tilde{\mathbf{s}}_{\text{in}}, \tilde{\mathbf{x}}_{\text{d}}\}$ as the training batch.
- 9: Update Θ_{FuSD} by using the Adam algorithm (learning rate γ_2) to minimize $\text{Loss}_{\text{FuSD-Net}}$.
- 10: **end for**

Testing phase:

- 11: Load the trained parameters Θ_{CE} and Θ_{FuSD} .
 - 12: Perform LS estimation to obtain $\hat{\mathbf{h}}_{\text{LS}}$ using Eq. (6).
 - 13: Reshape the complex-valued $\hat{\mathbf{h}}_{\text{LS}}$ to real-valued $\tilde{\mathbf{h}}_{\text{LS}}$ using Eq. (7).
 - 14: Predict $\tilde{\mathbf{h}}_{\text{CE}}$ based on Θ_{CE} and $\tilde{\mathbf{h}}_{\text{LS}}$ using Eq. (8).
 - 15: Perform ZF equalization to obtain $\hat{\mathbf{s}}_{\text{ZF}}$ using Eq. (10).
 - 16: Cancel the superimposed interference from pilot to obtain the coarse data $\hat{\mathbf{s}}_{\text{d}}$.
 - 17: Splice $\hat{\mathbf{s}}_{\text{d}}$ and \mathbf{y} to real-values using Eq. (13).
 - 18: Predict $\tilde{\mathbf{s}}_{\text{FuSD}}$ based on Θ_{FuSD} and $\tilde{\mathbf{s}}_{\text{in}}$ using Eq. (14).
-

the derivation process from the widely adopted COST2100 channel model [28]. The superimposed pilot \mathbf{x}_{p} is implemented using the Zadoff-Chu sequence, while the modulated signal \mathbf{x}_{d} is generated using a quadrature-phase-shift-keying (QPSK) symbol set [29]. According to (1)–(4), the set of received signal is formed as $\{\mathbf{y}\}$. Utilizing Eq. (6), we obtain the set $\{\hat{\mathbf{h}}_{\text{LS}}\}$. Subsequently, the complex-valued sets $\{\hat{\mathbf{h}}_{\text{Label}}\}$ and $\{\hat{\mathbf{h}}_{\text{LS}}\}$ are converted into the corresponding real-valued sets $\{\tilde{\mathbf{h}}_{\text{Label}}\}$ and $\{\tilde{\mathbf{h}}_{\text{LS}}\}$, respectively. The training process of LwCE-Net involves utilizing the training sets $\{\tilde{\mathbf{h}}_{\text{LS}}, \tilde{\mathbf{h}}_{\text{Label}}\}$. Algorithm 1 provides detailed insights into the methodology, outlining a comprehensive process. Moreover, during the training phase, a validation set is generated using the same method as the training set [29] to assess the performance of the trained network parameters.

The training criterion of the LwCE-Net is to minimize the mean squared error (MSE), and the corresponding loss function is expressed as follows

$$Loss_{\text{LwCE-Net}} = \frac{1}{S_1} \left\| \tilde{\mathbf{h}}_{\text{Label}} - \tilde{\mathbf{h}}_{\text{CE}} \right\|_2^2 + \beta_{\text{CE}} \sum_{\ell=2}^4 \left\| \mathbf{w}_{\text{CE}}^{(\ell)} \right\|_2^2, \quad (9)$$

where S_1 signifies the quantity of training samples, β_{CE} denotes the regularization coefficient employed to mitigate overfitting, and ℓ is the LwCE-Net layer index.

The training set, $\{\tilde{\mathbf{h}}_{\text{LS}}, \tilde{\mathbf{h}}_{\text{Label}}\}$, consists of 20,000 samples (while 100,000 samples are employed for the offline training in [19], [29]–[31]), with a batch size configured as 80 samples. This indicates that our lightweight NN can effectively reduce the size of the training set. The validation set for LwCE-Net contains 20,000 samples. We set the number of epochs for LwCE-Net to 40. For optimization, we employ the Adam optimizer based on [32] with the parameters $\beta_1 = 0.99$ and $\beta_2 = 0.999$ [33]. The learning rate is initially set to 0.001, and the L_2 regularization [34] is applied to the LwCE-Net.

The training phase involves a single execution of the training operation for LwCE-Net, after which the trained network is ready for online deployment.

3.3 Equalization Feature Extraction

To avoid relying on second-order noise statistics, initial equalization values derived from ZF equalization are incorporated as the input of FuSD-Net.

From Eq. (1), the pilot \mathbf{x}_p is superimposed onto the modulated signal \mathbf{x}_d . The received signal \mathbf{y} undergoes initial ZF equalization to emphasize the features relevant to SD. Leveraging the improved performance of LwCE-Net (i.e., $\hat{\mathbf{h}}_{\text{CE}}$) and the received signal \mathbf{y} , the ZF equalization is expressed as follows

$$\hat{\mathbf{s}}_{\text{ZF}} = \mathbf{G}_{\text{ZF}} \mathbf{y}, \quad (10)$$

where $\hat{\mathbf{s}}_{\text{ZF}}$ represents the initial symbol equalization, $\mathbf{G}_{\text{ZF}} \in \mathbb{C}^{N \times N}$ denotes the ZF equalization matrix, which is given by

$$\mathbf{G}_{\text{ZF}} = \text{diag} \left\{ \frac{1}{\hat{h}_{\text{CE}}(1)}, \frac{1}{\hat{h}_{\text{CE}}(2)}, \dots, \frac{1}{\hat{h}_{\text{CE}}(N)} \right\}, \quad (11)$$

where $\hat{h}_{\text{CE}}(n)$, $n = 1, 2, \dots, N$, is the n -th entry of $\hat{\mathbf{h}}_{\text{CE}}$.

According to (10), we obtain the superimposed data and pilot $\hat{\mathbf{s}}_{\text{ZF}}$. Subsequently, we remove the superimposed interference from the pilot signal, obtaining the coarse data $\hat{\mathbf{s}}_d$, which is expressed as

$$\hat{\mathbf{s}}_d = \hat{\mathbf{s}}_{\text{ZF}} - \sqrt{\lambda P} \mathbf{x}_p. \quad (12)$$

Then, the feature of the coarse data is extracted by referring to the obtained coarse data $\hat{\mathbf{s}}_d$, which will be used for subsequent recovery purposes.

3.4 Fusion Learning-based SD method

To enhance the accuracy of the coarse data $\hat{\mathbf{s}}_d$, we developed a lightweight FuSD-Net inspired by the concept of multimodal feature-level fusion. This network integrates the features extracted from the coarse data, obtained through the simplified equalization method using Eq. (12) with the received signal.

3.4.1 FuSD-Net Architecture

After the simplified ZF equalization, the lightweight FuSD-Net is utilized to enhance the detection performance. Similar to LwCE-Net, the architecture of FuSD-Net is presented in Table 1, based on extensive experimental investigations. FuSD-Net employs the same activation function as LwCE-Net [26]. Furthermore, BN is applied to normalize the input sets of FuSD-Net, ensuring a zero mean and unit variance of the network input. Table 1 provides a comprehensive overview of the architecture of the FuSD-Net, which is described as follows.

The input of the FuSD-Net, denoted as $\tilde{\mathbf{s}}_{in} \in \mathbb{R}^{4N \times 1}$, is formed by concatenating $\hat{\mathbf{s}}_d$ and \mathbf{y} , i.e.,

$$\tilde{\mathbf{s}}_{in} = [\text{Re}(\hat{\mathbf{s}}_d^T), \text{Im}(\hat{\mathbf{s}}_d^T), \text{Re}(\mathbf{y}^T), \text{Im}(\mathbf{y}^T)]^T. \quad (13)$$

Next, the output $\tilde{\mathbf{s}}_{FuSD}$ is obtained through the utilization of the FuSD-Net by

$$\tilde{\mathbf{s}}_{FuSD} = f_{FuSD}(\tilde{\mathbf{s}}_{in}, \mathbf{\Lambda}_{FuSD}), \quad (14)$$

where $f_{FuSD}(\cdot)$ represents the fusion network operation, and $\mathbf{\Lambda}_{FuSD}$ denotes its network parameters.

3.4.2 Training and Deployment

Similar to the training process of LwCE-Net, a collection of data samples is gathered to train the FuSD-Net. The details of the training process are elaborated as follows.

According to Eq. (13), the input of FuSD-Net, denoted as $\tilde{\mathbf{s}}_{in}$, is utilized to construct the real-valued fusion set, represented as $\{\tilde{\mathbf{s}}_{in}\}$. Subsequently, the real-valued sets $\{\tilde{\mathbf{s}}_{in}, \tilde{\mathbf{x}}_d\}$ are formed by combining the training sets of $\{\tilde{\mathbf{s}}_{in}\}$ and $\{\tilde{\mathbf{x}}_d\}$ for training the FuSD-Net. The specific details of this process are elaborated in Algorithm 1. In addition, a validation set is also required. The loss function of FuSD-Net can be expressed as

$$Loss_{FuSD-Net} = \frac{1}{S_2} \|\tilde{\mathbf{x}}_d - \tilde{\mathbf{s}}_{in}\|_2^2 + \beta_{FuSD} \sum_{r=2}^3 \left\| \mathbf{W}_{FuSD}^{(r)} \right\|_2^2, \quad (15)$$

where S_2 denotes the number of training sets utilized for FuSD-Net, β_{FuSD} represents the regularization coefficient of FuSD-Net, and r indicates the network layer index.

The training sets, $\{\tilde{\mathbf{s}}_{in}, \tilde{\mathbf{x}}_d\}$, consist of 20,000 samples, wherein 100,000 samples are employed for the offline training in [19], [29]–[31]. The proposed lightweight NN reduces the size of the training dataset. The batch size is set to 80, and the validation sets for FuSD-Net contain 20,000 samples. Training is conducted for a total of 100 epochs.

The FuSD-Net adopts the same network parameter settings as LwCE-Net. During the training process of FuSD-Net, the training samples are generated by randomly selecting SNRs from 0 dB to 18 dB.

3.5 Online Deployment

Algorithm 1 outlines the procedure for online deployment, utilizing the trained network parameters obtained from offline training for LwCE-Net and FuSD-Net. The following provides a detailed explanation of Algorithm 1.

During the online running, the received signal \mathbf{y} and the known pilot \mathbf{x}_p are utilized to perform the LS estimation using Eq. (6). The initial estimation $\hat{\mathbf{h}}_{LS}$ is used as input for LwCE-Net, which generates $\tilde{\mathbf{h}}_{LS}$ by using Eq. (7). The LwCE-Net further refines $\tilde{\mathbf{h}}_{LS}$ to obtain the real-valued refined estimation feature $\tilde{\mathbf{h}}_{CE}$ (Eq. (8)). The complex-valued estimation feature $\hat{\mathbf{h}}_{CE}$ is obtained by extracting the real and imaginary parts from $\tilde{\mathbf{h}}_{CE}$, i.e.,

$$\begin{cases} \text{Re}(\hat{\mathbf{h}}_{CE}) = \tilde{\mathbf{h}}_{CE}(1:N) \\ \text{Im}(\hat{\mathbf{h}}_{CE}) = \tilde{\mathbf{h}}_{CE}(N+1:2N) \end{cases}, \quad (16)$$

The real part of $\hat{\mathbf{h}}_{CE}$ is formed by extracting the first N entries of $\tilde{\mathbf{h}}_{CE}$, while the imaginary part is composed of the last N entries. Using the estimated $\hat{\mathbf{h}}_{CE}$, ZF equalization is applied using Eq. (10) to obtain $\hat{\mathbf{s}}_{ZF}$. Subsequently, the superimposed interference is canceled, yielding the coarse data $\hat{\mathbf{s}}_d$ with Eq. (12). By combining the complex-valued $\hat{\mathbf{s}}_d$ and \mathbf{y} using Eq. (13), the real-valued $\tilde{\mathbf{s}}_{in}$ is formed. The FuSD-Net then utilizes $\tilde{\mathbf{s}}_{in}$ as the network input, combining the coarse data feature and received signal \mathbf{y} through feature fusion. Finally, the FuSD-Net employs Eq. (14) to output the detected symbol $\tilde{\mathbf{s}}_{FuSD}$.

Based on the algorithm outlined in our work (Algorithm 1), the refined detection output, $\tilde{\mathbf{s}}_{FuSD}$, can be obtained by utilizing the proposed architectures of LwCE-Net and FuSD-Net. The integration of FuSD-Net allows for high-precision detection of $\tilde{\mathbf{s}}_{FuSD}$. In comparison to conventional estimation methods like MMSE CE and MMSE SD, the proposed approach demonstrates superior detection performance, as evidenced by its lower BER performance. It is noteworthy that the performance of the proposed method is refined without any second-order statistic of wireless noise and channel.

Remark1: Battery Life and Spectral Efficiency

In comparison to IoT systems that do not employ superimposed pilot and RIS, the proposed method in this paper offers significant enhancements in the battery life of UE and the spectral efficiency of the IoT system. The adoption of the superimposition mode leads to a substantial reduction in energy consumption for IoT UEs, even under the same transmitted power. Additionally, the inclusion of RIS improves communication reliability, resulting in enhanced energy efficiency while maintaining comparable communication quality when compared to IoT systems without RIS. In the context of an IoT system operating with limited bandwidth, the utilization of superimposed pilots, as proposed in this paper, effectively boosts spectral efficiency. Consequently, the proposed method of superimposed pilot-based CE with RIS assistance offers notable advantages over IoT systems that do not employ superimposed pilot and RIS.

Specifically, it effectively extends the battery life of UEs and enhances the spectral efficiency of IoT systems, leading to substantial improvements in performance.

The proposed method employs the superimposed pilot mode, which eliminates the need for additional resources for pilot transmission by the UE. As a result, the proposed method achieves enhanced spectral efficiency compared to CE methods that do not employ superimposed pilot techniques [6], [7]. Furthermore, by eliminating the need for additional energy for pilot transmission, the proposed method reduces energy consumption at the UE. Table 2 presents a comparison of the bandwidth resource utilization and energy consumption between the non-superimposed pilot-based CE method [6], [7] and the proposed method outlined in this paper.

The energy consumption of the non-superimposed pilot-based CE method can be denoted as

$$E_{\text{NonSup}} = (N_{\text{data}} + N_{\text{Pilot}}) T_0 P, \quad (17)$$

where N_{data} represents the total number of data symbols, N_{Pilot} signifies the count of pilot symbols, T_0 indicates the duration of each symbol, and P is the transmission power.

Table 2

Bandwidth resource occupation and energy consumption.

Method	Bandwidth resource usage		Total energy consumption	
	Expression	Example	Expression	Example
Non-superimposed pilot	$(N_{\text{data}} + N_{\text{Pilot}}) T_0$	$64T_0$	$(N_{\text{data}} + N_{\text{Pilot}}) T_0 P$	$64T_0 P_0$
Superimposed pilot	$(N_{\text{data}}) T_0$	$32T_0$	$N_{\text{data}} T_0 ((1-\lambda) P) + N_{\text{Pilot}} T_0 (\lambda P)$	$32T_0 P_0$

Compared with the CE method based on non-superimposed pilots [6], [7], the adoption of the superimposed pilot mode in the proposed method reduces energy consumption at the UE, as it eliminates the need for additional energy expenditure in pilot transmission. In this paper, the energy consumption of the proposed scheme is denoted as E_{Prop} , which is expressed as

$$E_{\text{Prop}} = N_{\text{data}} T_0 ((1-\lambda) P) + N_{\text{Pilot}} T_0 (\lambda P), \quad (18)$$

where λ denotes the proportional coefficient of power. Compared with the non-superimposed pilot-based CE, the energy saving by using the proposed method could be calculated as

$$E_{\text{NonSup}} - E_{\text{Prop}} = N_{\text{data}} T_0 (\lambda P) + N_{\text{Pilot}} T_0 ((1-\lambda) P). \quad (19)$$

In terms of bandwidth resource occupation, the proposed method utilizes a superimposed pilot transmission approach, resulting in a time duration of $N_{\text{data}} T_0$. In contrast, the non-superimposed pilot-based CE method occupies a bandwidth resource for a duration of $(N_{\text{data}} + N_{\text{Pilot}}) T_0$. Therefore, the proposed method

reduces the bandwidth resource occupation compared to the non-superimposed pilot-based CE, leading to a reduction in the bandwidth resource occupation denoted as $(N_{\text{data}} + N_{\text{Pilot}})T_0 - N_{\text{data}}T_0 = N_{\text{Pilot}}T_0$. By considering the case where $N_{\text{data}} = 32$ and $N_{\text{Pilot}} = 32$, as shown in Table 2, it is evident that the proposed method significantly reduces both the bandwidth resource occupation and energy consumption compared to the CE method based on non-superimposed pilot. In summary, the proposed method enhances the spectral and energy efficiency of RIS-assisted IoT systems when compared to non-superimposed pilot-based CE methods.

In addition to the advantages mentioned in *Remark 1*, the proposed superimposed pilot-based CE with RIS assistance also reduces the computational complexity and processing delay at the BS, compared to IoT systems that do not employ superimposed pilot and RIS. The comprehensive analysis and comparison of the computational complexity and processing delay at the BS are presented in Section 4.

4 Complexity and Running Time Analyses

For convenience, the simplified expression is as follows.

- “LS-CE”, “MMSE-CE” and “LwCE-Net” are used to represent the “LS channel estimation”, “MMSE channel estimation”, and “proposed LwCE-Net”, respectively.
- “MMSE-CE + MMSE-SD”, “LwCE-Net + ZF” and “proposed” are utilized to stand the “MMSE channel estimation followed by MMSE equalization”, “proposed LwCE-Net followed by ZF equalization”, and “proposed LwCE-Net followed by FuSD-Net”, respectively.

4.1 Computational complexity

The computational complexity of NNs is commonly assessed based on the number of weights and floating-point operations (FLOPs) [31], which serve as widely used criteria. In this paper, we evaluate the computational complexity using these criteria and present a detailed analysis in Table 3. The specifics are outlined as follows.

According to the computation method described in [31], the proposed LwCE-Net and FuSD-Net have a total of $28N^2 + 8N$ weights and require $56N^2 - 8N$ FLOPs. Consequently, the proposed method, including both LwCE-Net and FuSD-Net, achieves a reduced computational complexity, i.e., $28N^2 + 8N + 56N^2 - 8N = 84N^2$. This is significantly lower than the computational complexity of the “MMSE-CE + MMSE-SD” method. Table 3 provides a clear comparison of the computational complexities, highlighting the advantages of the proposed method. For the case where $N = 32$, i.e., case 1 in Table 3, the computational complexity of the “MMSE-CE + MMSE-SD” is 200,768, whereas the computational complexity of the “proposed” is 86,016. When $N = 64$ (i.e., case 2 in Table 3), the computational complexity of the “MMSE-CE + MMSE-SD” is 1,589,376, while the computational complexity of the “proposed” is 344,064. On the whole, compared with the “MMSE-CE + MMSE-SD”, the proposed method reduces the complexity of computation and thus obtains the corresponding improvement for energy consumption.

Table 3
the Analysis of computational complexity.

Method	proposed	MMSE-CE + MMSE-SD
Complexity	$84N^2$	$6N^3 + 4N^2 + 2N$
Case 1 ($N = 32$)	86,016	200,768
Case 2 ($N = 64$)	344,064	1,589,376

4.2 Running Time

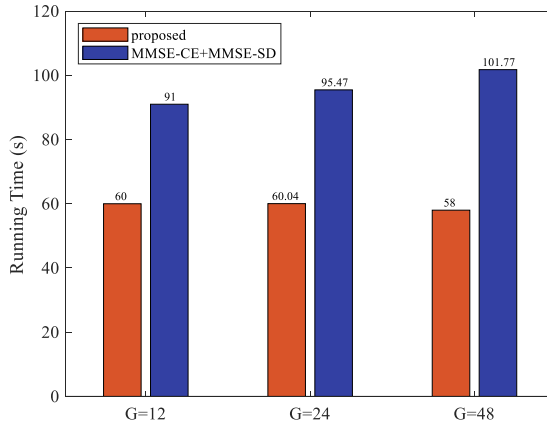


Fig. 2 Running time comparison of “proposed”, and “MMSE-CE+MMSE-SD” for 3×10^4 experiments, where $G = 12$, $G = 24$, and $G = 48$ are discussed.

The proposed method was trained on a server with an Intel Xeon(R) E5-2620 CPU (2.1GHz×16). MATLAB simulations were conducted on the server CPU to obtain the results since a GPU-based solution for the “MMSE-CE + MMSE-SD” was not available. The running time details are discussed in Fig. 2. In the case where $G = 12$, the proposed method takes approximately 60 seconds for both LwCE-Net and FuSD-Net. In contrast, the “MMSE-CE + MMSE-SD” method requires about 91 seconds. These findings demonstrate that the proposed method has a shorter online running time and contributes to prolonging the battery life of the UE.

Thus, compared with the “MMSE-CE + MMSE-SD”, the “proposed” significantly reduces their computational complexity and running time.

5 Simulation Results and Analysis

In this section, we present numerical results for the proposed method. Section 5.1 introduces the simulation parameters and definitions. Section 5.2 presents the

simulation results to validate the proposed method. Lastly, Section 5.3 analyzes the robustness of the parameters.

5.1 Parameters and Definitions

In all conducted experiments, unless explicitly stated, the following fundamental parameters are employed. The pilot is Zadoff-Chu sequence [23], $L = 5$, $N = 32$, $\lambda = 0.15$, and $G = 12$. The channel is based on the COST2100 model [28], and the transmitted data symbol is modulated with QPSK¹. The signal-to-noise ratio (SNR) is expressed in decibel (dB) [35]

$$\text{SNR} = 10\log_{10} \left(\frac{P}{\sigma_w^2} \right), \quad (20)$$

where P represents the aggregate transmitted power comprising both the data power P_d and pilot power P_p . In these simulations, $P_d = 0.85P$ and $P_p = 0.15P$.

The NMSE is utilized to evaluate the CE performance, defined as [35]

$$\text{NMSE} = E \left\{ \frac{\|\hat{\mathbf{h}}_{\text{CE}} - \mathbf{h}\|_2^2}{\|\mathbf{h}\|_2^2} \right\}. \quad (21)$$

5.2 NMSE Analysis

As shown in Fig. 3, we demonstrate the effectiveness of the proposed LwCE-Net through the NMSE curves, that the values of NMSE of “LS-CE” and “MMSE-CE” are much higher than that of the “LwCE-Net” for all given SNRs. For example, the NMSE of the “LwCE-Net” is less than 1×10^{-2} for the case of SNR = 18 dB, while the NMSE of the “MMSE-CE” is 2×10^{-1} and “LS-CE” is higher than 1×10^0 at the same SNR. The reason of the poor performance of the “LS-CE” is that the LS estimation is sensitive to the noise and interference. The superimposed pilot is equivalent to introducing the superimposed interference, which results in an unsatisfactory LS estimation. However, the NMSE of “MMSE-CE” is still unsatisfying due to the influence of superimposed interference. In contrast, the developed LwCE-Net effectively alleviates the impact of superimposed interference by exploiting its learning ability of de-noising (suppressing the superimposed interference and noise) and feature extraction (learning the feature of wireless channels). Thus, compared with the linear solution estimated by LS and MMSE-based CE, the developed LwCE-Net learns a nonlinear solution orienting the LS solution, which enhances the NMSE performance of the CE.

¹The modulation with a higher modulation order is also suitable for the proposed method.

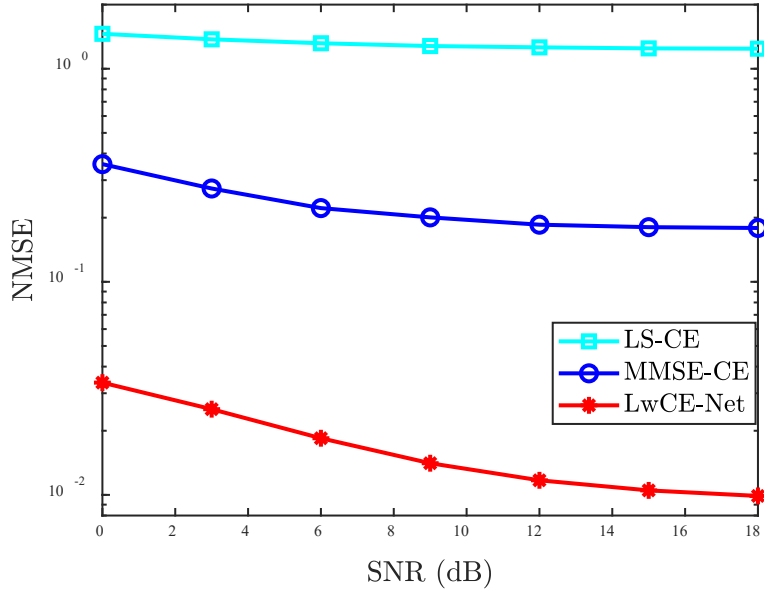


Fig. 3 NMSE comparison of “LS-CE”, “MMSE-CE”, “LwCE-Net”, where SNR varies from 0 to 18 dB.

5.3 BER Analysis

To evaluate the impact of the superimposed interference caused by the pilot \mathbf{x}_p on the detection performance of the modulated symbol \mathbf{x}_d , we utilize the bit error rate (BER) as a metric. The BER results are presented in Fig. 4. We compare the proposed method with the baseline methods “MMSE-CE+MMSE-SD” and “LwCE-Net+ZF” to evaluate their BER. As shown in Fig. 4, the BER of the “proposed” is much smaller than that of the “MMSE-CE+MMSE-SD”. For example, for the case where SNR = 14dB, the BER of the “proposed” is less than 1×10^{-2} while the BER of the “MMSE-CE+MMSE-SD” is about 6.5×10^{-2} . Furthermore, the BER of the “LwCE-Net+ZF” is smaller than that of the “MMSE-CE+MMSE-SD”. One of the main reasons is that the poor NMSE performance of the “MMSE-CE+MMSE-SD” affects the subsequent detection performance. The error of CE is propagated to the detection stage and thus degrades the detection performance of the “MMSE-CE+MMSE-SD”.

With the superior learning ability of the LwCE-Net, the NMSE performance of the “proposed” is improved by the LwCE-Net, to improve its BER performance. At the same time, we can see that the “proposed” achieves a smaller value of BER than the “LwCE-Net+ZF”. For example, when SNR = 18 dB, the BER of the “proposed” is 1.2×10^{-3} while the BER of the “LwCE-Net+ZF” reaches 5×10^{-3} . Because there is an additional data fusion network FuSD-Net in the “proposed”, it is more powerful to capture additional features for SD and thus effectively improve its BER performance.

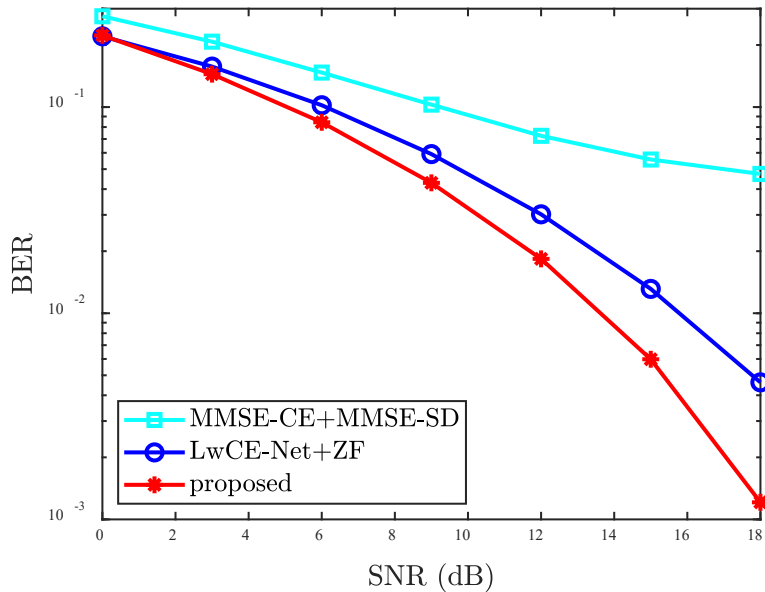


Fig. 4 BER comparison of “proposed”, “MMSE-CE+MMSE-SD”, “LwCE-Net+ZF”, where SNR varies from 0 to 18 dB.

5.4 Robustness Analysis

This subsection examines the robustness of the proposed method to parameter variations, specifically the power proportional coefficient λ and the number of multipaths L . For ease of analysis, we vary one parameter at a time while keeping other fundamental parameters unchanged, as outlined in Section 5.1.

5.4.1 Robustness against λ

In general, different power proportional coefficient λ will result in different performance of CE and SD for the superimposed signals. Fig. 5 illustrates the NMSE of CE and the BER of SD to demonstrate the robustness of the “proposed” method against variations in λ .

From Fig. 5, as the increase of λ (increase from 0.1 to 0.2), the CE’s NMSEs of “LS-CE” and “MMSE-CE” decrease. Although the decline of NMSE is not obvious, the decreasing trend is still observed. For example, when SNR = 12dB and λ changes from 0.1 to 0.2, the “MMSE-CE” changes from 3×10^{-1} to 1.2×10^{-1} . The likely reason is that the CE performance is improved due to the increased pilot power. Meanwhile the NMSE performance of the “proposed” remains stable and is smaller than “LS-CE” and “MMSE-CE” with the increase of λ . For example, for the case where SNR = 12dB and $\lambda = 0.15$, the values of NMSE are higher than 1×10^0 and 2×10^{-1} for “LS-CE” and “MMSE-CE”, respectively. By contrast, the NMSE of the “proposed” is about 1×10^{-2} .

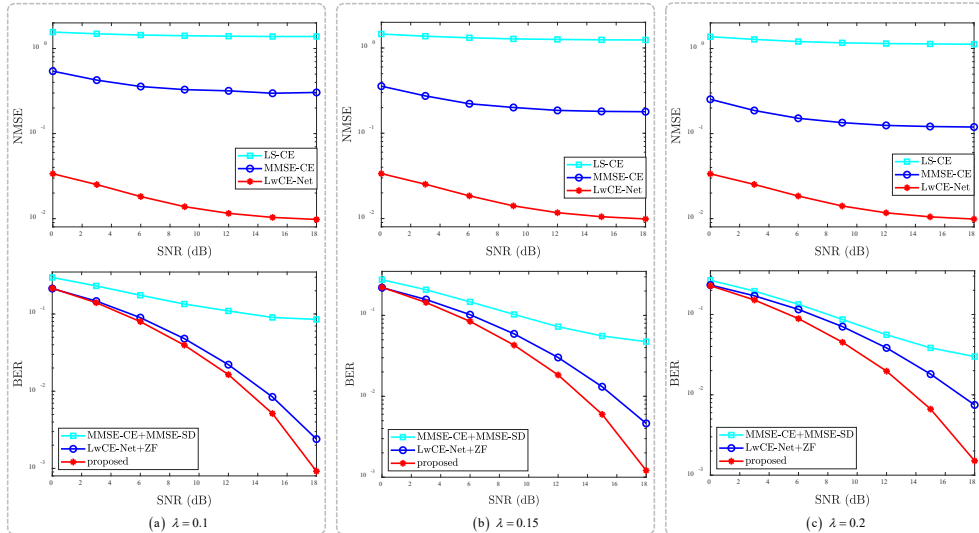


Fig. 5 NMSE and BER performance against the impact of λ , where $\lambda = 0.1$, $\lambda = 0.15$, and $\lambda = 0.2$ are considered, respectively.

With the increase of λ , the BER performance of the “LwCE-Net+ZF” and “proposed” deteriorate slightly. For example, for the case where SNR = 18 dB and $\lambda = 0.1$, the values of BER are about 2.2×10^{-3} and 1×10^{-3} , respectively. While for the case where SNR = 18 dB and $\lambda = 0.2$, the values of BER are about 8×10^{-3} and 2×10^{-3} , respectively. However, the BER of the “proposed” remains much smaller than those of “LwCE-Net+ZF” and “MMSE-CE+MMSE-SD” for each given SNR and λ . Thus, against the impact of λ , the “proposed” improves the BER performance when compared with the “LwCE-Net+ZF” and “MMSE-CE+MMSE-SD”.

On the whole, when compared with the “LwCE-Net+ZF” and “MMSE-CE+MMSE-SD”, the “proposed” enhances the NMSE and BER performance against the variation of λ .

5.4.2 Robustness against L

As shown in Fig. 6, it demonstrates the robustness of the “proposed” method against variations in the number of multi-path, i.e., L , by comparing its performance. The varying of NMSE is not regular with the enlargement of L . The reason is that the performance of NMSE is not so directly related to the values of L . Even so, we can see that no matter how the values of L change, using the “LwCE-Net” achieves the minimum value of NMSE, presenting the best NMSE performance. For example, when SNR = 12dB and $L = 5$, the NMSE values of “LS-CE” and “MMSE-CE” are respectively higher than 1×10^0 and 2×10^{-1} , while the NMSE of “LwCE-Net” is about 1.2×10^{-2} . This reflects that the LwCE-Net improves the NMSE performance

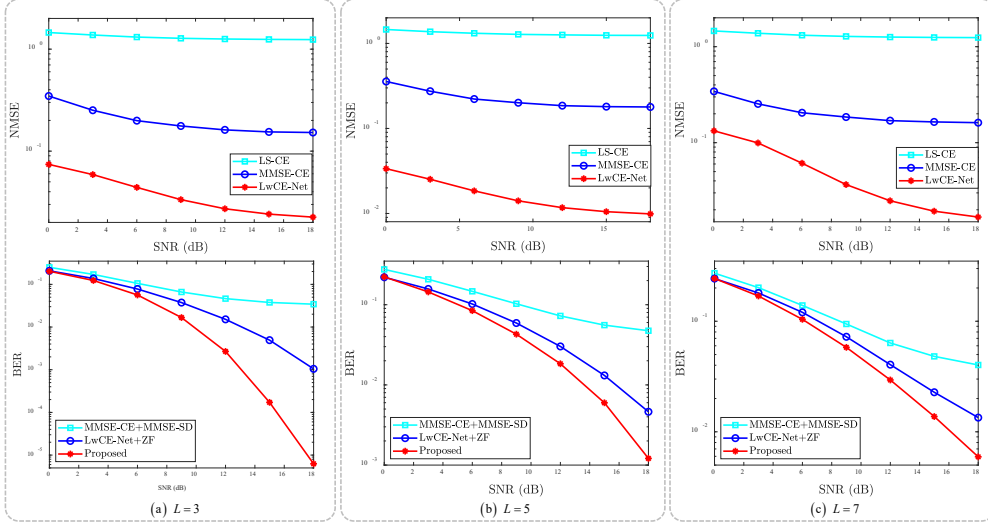


Fig. 6 NMSE and BER performance against the impact of L , where $L = 3$, $L = 5$, and $L = 7$ are considered, respectively.

compared with the conventional methods of “LS-CE” and “MMSE-CE” against the variations of L .

Besides, from Fig. 6, compared with the “MMSE-CE+MMSE-SD” and “CE-Net+ZF”, the “proposed” achieves smaller BER for each given L . For example, for the cases of SNR = 18 dB and $L = 5$, BERs of the “MMSE-CE+MMSE-SD” and “LwCE-Net+ZF” are about 5.5×10^{-2} and 4.5×10^{-3} respectively, while the BER of “proposed” is smaller than 2×10^{-3} . This reflects that the “proposed” improves the BER compared with the “MMSE-CE+MMSE-SD” and “LwCE-Net+ZF” against the variation of L . Besides, it is worth noting that for the case of $L = 5$, each of the CE methods achieves the smallest NMSE, yet they cannot achieve the best detection performance. This is because in the case of superimposed pilots, although the estimation performance is improved, the detection performance is not necessarily improved proportionally due to the influence of superimposed interference. Thus, an effective option is to make a tradeoff between NMSE performance and BER performance for the superimposed pilot-based method.

Therefore, against the impact of L , Fig. 6 shows that both of the NMSE and BER performance are improved by “proposed” when compared with the “LwCE-Net+ZF” and “MMSE-CE+MMSE-SD”.

6 Conclusion

This paper proposes a superimposed pilot-based CE technique in RIS-assisted mode for IoT systems. By employing superimposed pilot, we enhance spectral efficiency and

reduce energy consumption, while the deployment of RIS mitigates blocked propagation paths. Additionally, we integrate both non-NN and NN based modes at the BS, resulting in lightweight networks that effectively reduce computational complexity and processing delays. The proposed solution demonstrates significant and robust improvements in NMSE and BER performance compared to conventional methods. In our forthcoming research endeavors, we will undertake an in-depth investigation into the influence of RIS materials on CE.

Declarations

- Conflict of interest

The authors declare the following financial interests/personal relationships which may be considered as potential competing interests:

This work is supported in part by the Sichuan Science and Technology Program (Grant No. 2023YFG0316), the Industry-University Research Innovation Fund of China University (Grant No. 2021ITA10016), the Key Scientific Research Fund of Xihua University (Grant No. Z1320929), and the Special Funds of Industry Development of Sichuan Province (Grant No. zyf-2018-056).

- Author Agreement

Dear Editor:

We would like to submit the enclosed manuscript entitled "Superimposed Pilot-based Channel Estimation for RIS-Assisted IoT systems Using Lightweight Networks", which we wish to be considered for publication in "Wireless Personal Communications". No conflict of interest exists in the submission of this manuscript, and the manuscript is approved by all authors for publication. I would like to declare on behalf of my co-authors that the work described was original research that has not been published previously, and not under consideration for publication elsewhere, in whole or in part. All the authors listed have approved the manuscript that is enclosed.

Thank you and best regards.

Yours sincerely,

Chaojin Qing

Corresponding author: Chaojin Qing (qingchj@mail.xhu.edu.cn)

References

- [1] T. Jiang, Y. Shi, J. Zhang, and K. Letaief, "Joint activity detection and channel estimation for IoT networks: Phase transition and computation-estimation tradeoff," *IEEE Internet Things J.*, vol. 6, no. 4, pp. 6212–6225, Aug. 2019.
- [2] X. Wu, X. Yang, S. Ma, B. Zhou, and G. Yang, "Hybrid channel estimation for UPA-assisted millimeter-wave massive MIMO IoT systems," *IEEE Internet Things J.*, pp. 1–1, July 2021.

- [3] Z. Zhang, Y. Li, C. Huang, Q. Guo, L. Liu, C. Yuen, and Y. Guan, "User activity detection and channel estimation for grant-free random access in LEO satellite-enabled internet of things," *IEEE Internet Things J.*, vol. 7, no. 9, pp. 8811–8825, Sep. 2020.
- [4] M. Jewel, R. Zakariyya, and F. Lin, "A pilot-based hybrid and reduced complexity channel estimation method for downlink NB-IoT systems," in *Proc. IEEE MTT-S International Wireless Symposium*, Sep. 2020, pp. 1–3.
- [5] P. Liu and T. Jiang, "Channel estimation performance analysis of massive MIMO IoT systems with ricean fading," *IEEE Internet Things J.*, vol. 8, no. 7, pp. 6114–6126, Apr. 2021.
- [6] M. Ali, Y. Li, M. Jewel, O. Famoriji, and F. Lin, "Channel estimation and peak-to-average power ratio analysis of narrowband internet of things uplink systems," *Wireless Commun. Mobile Comput.*, vol. 2018.
- [7] M. Jewel, R. Zakariyya, O. Famoriji, M. Ali, and F. Lin, "A low complexity channel estimation technique for NB-IoT downlink system," in *Proc. IEEE MTT-S International Wireless Symposium*, May 2019, pp. 1–3.
- [8] M. Ali, M. Jewel, and F. Lin, "An efficient channel estimation technique in NB-IoT systems," in *Proc. IEEE International Conf. Integrated Circuits, Techn. Applications*, Nov. 2018, pp. 22–23.
- [9] J. Won and J. Ahn, "NB-IoT downlink channel estimation," in *Proc. International Conf. Information Communi. Techn. Convergence*, Oct. 2020, pp. 1739–1741.
- [10] Y. You, Y. Jung, S. Choi, and I. Hwang, "Complexity-effective sequential detection of synchronization signal for cellular narrowband IoT communication systems," *IEEE Internet Things J.*, vol. 8, no. 4, pp. 2900–2909, Feb. 2021.
- [11] J. Jiao, J. Zhou, S. Wu, and Q. Zhang, "Superimposed pilot code-domain NOMA scheme for satellite-based internet of things," *IEEE Syst. J.*, vol. 15, no. 2, pp. 2732–2743, June 2021.
- [12] Z. Mao, M. Peng, and X. Liu, "Channel estimation for reconfigurable intelligent surface assisted wireless communication systems in mobility scenarios," *China Commun.*, vol. 18, no. 3, pp. 29–38, Mar. 2021.
- [13] Q. Wu and R. Zhang, "Towards smart and reconfigurable environment: Intelligent reflecting surface aided wireless network," *IEEE Commun. Mag.*, vol. 58, no. 1, pp. 106–112, Jan. 2020.
- [14] G. Alexandropoulos and E. Vlachos, "A hardware architecture for reconfigurable intelligent surfaces with minimal active elements for explicit channel estimation,"

- in *Proc. IEEE Int. Conf. Acoust., Speech Signal Process.*, May 2020, pp. 9175–9179.
- [15] C. Huang, A. Zappone, M. Debbah, and C. Yuen, “Achievable rate maximization by passive intelligent mirrors,” in *Proc. IEEE Int. Conf. Acoust., Speech Signal Process.*, Apr. 2018, pp. 3714–3718.
- [16] R. Shaddad, E. Saif, H. Saif, Z. Mohammed, and A. Farhan, “Channel estimation for intelligent reflecting surface in 6G wireless network via deep learning technique,” in *Proc. Int. Conf. Emerging Smart Technol. Appl.*, Aug. 2021, pp. 1–5.
- [17] T. Wang, C. Wen, H. Wang, F. Gao, T. Jiang, and S. Jin, “Deep learning for wireless physical layer: Opportunities and challenges,” *China Commun.*, vol. 14, no. 11, pp. 92–111, Dec. 2017.
- [18] Y. Fan, D. Dan, Y. Li, Z. Wang, and Z. Liu, “Intelligent communication: Application of deep learning at the physical layer of communication,” in *Proc. IEEE Adv. Inf. Manag., Commun., Electron. Autom. Control Conf.*, vol. 4, July 2021, pp. 1339–1345.
- [19] N. Kundu and M. McKay, “Channel estimation for reconfigurable intelligent surface aided MISO communications: From LMMSE to deep learning solutions,” *IEEE Open J. Commun. S.*, vol. 2, pp. 471–487, Mar. 2021.
- [20] C. Qing, L. Wang, L. Dong, and J. Wang, “Enhanced ELM based channel estimation for RIS-assisted OFDM systems with insufficient CP and imperfect hardware,” *IEEE Commun. Lett.*, pp. 1–1, Oct. 2021.
- [21] N. Ginige, K. Manosha, N. Rajatheva, and M. Latva-aho, “Untrained DNN for channel estimation of RIS-assisted multi-user OFDM system with hardware impairments,” in *Proc. IEEE Annual International Symposium Pers., Indoor Mobile Radio Commun.*, Oct. 2021, pp. 561–566.
- [22] M. Ali, Y. Li, M. Jewel, O. Famoriji, and F. Lin, “Channel estimation and peak-to-average power ratio analysis of narrowband internet of things uplink systems,” *Wireless Commun. Mobile Computing*, vol. 2018.
- [23] B. Zheng and R. Zhang, “Intelligent reflecting surface-enhanced OFDM: Channel estimation and reflection optimization,” *IEEE Wireless Commun. Lett.*, vol. 9, no. 4, pp. 518–522, Apr. 2020.
- [24] C. He, G. Huang, J. Gao, G. Dou, and W. Ying, “Semiblind channel estimation and symbol detection for block transmission using superimposed training,” in *Proc. IEEE Int. Conf. Computer Inf. Technol.*, Oct. 2012, pp. 627–630.

- [25] A. Zappone, M. Renzo, and M. Debbah, “Wireless networks design in the era of deep learning: Model-based, AI-based, or both?” *IEEE Trans. Commun.*, vol. 67, no. 10, pp. 7331–7376, Oct. 2019.
- [26] S. Ioffe and C. Szegedy, “Batch normalization: accelerating deep network training by reducing internal covariate shift,” in *Proc. Int. Conf. Mach. Learn.*, Mar. 2015, pp. 448–456.
- [27] H. Huang, W. Xia, J. Xiong, J. Yang, G. Zheng, and X. Zhu, “Unsupervised learning-based fast beamforming design for downlink MIMO,” *IEEE Access*, vol. 7, pp. 7599–7605, Dec. 2019.
- [28] L. Liu, C. Oestges, J. Poutanen, K. Haneda, P. Vainikainen, F. Quitin, F. Tufveson, and P. Doncker, “The COST 2100 MIMO channel model,” *IEEE Wireless Commun.*, vol. 19, no. 6, pp. 92–99, Dec. 2012.
- [29] C. Qing, L. Dong, L. Wang, J. Wang, and C. Huang, “Joint model and data driven receiver design for data-dependent superimposed training scheme with imperfect hardware,” *IEEE Trans. Wireless Commun.*, pp. 1–1, Nov. 2021.
- [30] Y. Enku, B. Bai, F. Wan, C. Guyo, I. Tiba, C. Zhang, and S. Li, “Two-dimensional convolutional neural network-based signal detection for OTFS systems,” *IEEE Wireless Commun. Lett.*, vol. 10, no. 11, pp. 2514–2518, 2021.
- [31] J. Guo, C. Wen, and S. Jin, “CANet: Uplink-aided downlink channel acquisition in FDD massive MIMO using deep learning,” *IEEE Trans. Commun.*, vol. 70, no. 1, pp. 199–214, Jan. 2022.
- [32] D. Kingma and J. Ba, “Adam: a method for stochastic optimization,” 2014, *arXiv:1412.6980*. [Online]. Available: <https://arxiv.org/abs/1412.6980>.
- [33] V. Raj and S. Kalyani, “Backpropagating through the air: Deep learning at physical layer without channel models,” *IEEE Commun. Lett.*, vol. 22, no. 11, pp. 2278–2281, Nov. 2018.
- [34] I. Goodfellow, Y. Bengio, and A. Courville, *Deep learning*, 2016.
- [35] C. Qing, B. Cai, Q. Yang, J. Wang, and C. Huang, “Elm-based superimposed csi feedback for fdd massive mimo system,” *IEEE Access*, vol. 8, pp. 53 408–53 418, 2020.